Available online at www.sciencedirect.com

SciVerse ScienceDirect

Scripta Materialia 68 (2013) 348–353

Scripta MATERIALIA

www.elsevier.com/locate/scriptamat

Viewpoint Paper

Direct evidence for the formation of ordered carbides in a ferrite-based low-density Fe–Mn–Al–C alloy studied by transmission electron microscopy and atom probe tomography

Jae-Bok Seol,[a] Dierk Raabe,[a] P. Choi,[a] Hyung-Seok Park,[b] J.-H. Kwak[c] and Chan-Gyung Park[b,*]

[a] *Max-Planck-Insititut für Eisenforschung, Max-Planck-Str.1, 40237 Düsseldorf, Germany*
[b] *Materials Science and Engineering, POSTECH, Pohang 790-784, Republic of Korea*
[c] *Automotive Steels Research Laboratories, POSCO, Gwangyang 545-711, Republic of Korea*

Available online 17 August 2012

Abstract—We study the structure and chemical composition of the κ-carbide formed as a result of isothermal transformation in an Fe–3.0Mn–5.5Al–0.3C alloy using transmission electron microscopy and atom probe tomography. Both methods reveal the evolution of κ-particle morphology as well as the partitioning of solutes. We propose that the κ-phase is formed by a eutectoid reaction associated with nucleation growth. The nucleation of κ-carbide is controlled by both the ordering of Al partitioned to austenite and the carbon diffusion at elevated temperatures.

Keywords: Lightweight steels; Ordered carbide; Decomposition; Atom probe tomography

1. Introduction

Recent trends in designing advanced high-strength steels aim at controlling the mechanical properties and reducing the specific weight by varying the Mn and Al contents [1–6]. Following this concept, a ferritic-matrix-based Fe–Mn–Al–C alloy with a higher content of Al than Mn was developed [7]. The major benefit behind this alloy design is a weight reduction of ~10% compared to transformation-induced plasticity or twinning induced plasticity steels. The reduction in mass density is due to the high Al content, which also enhances oxidation, corrosion resistance and impact toughness at high temperature [6,8]. These new low-density steels can achieve tensile strengths above 780 MPa and elongations above 30% owing to the formation of the ordered $L'1_2$ κ-carbide, $(Fe,Mn)_3AlC_x$ [8]. The deformation behavior of weight-reduced austenitic Fe–Mn–Al–C alloys is reported to depend on the size, fraction, location and distribution of the κ-phase [9–11]. However, no experimental investigations have so far been made on the compositional gradients across the phase boundaries between κ-carbide and abutting phase, except for an austenitic Fe–(20–30)Mn–Al–C alloy (wt.%) using electron probe microanalysis at the micrometer-scale [12,13]. Moreover, the effects of isothermal annealing on the precipitation of the κ-phase in Fe–Mn–Al–C alloys have not yet been elucidated.

The present study aims at identifying the decomposition mechanism of metastable austenite into ferrite and κ-carbide upon isothermal annealing in high-Al steels from the viewpoint of experiments and thermodynamic calculations. Using transmission electron microscopy (TEM), the present study gives detailed information on κ-carbide, such as crystallographic structure, morphology and orientation relationship with the abutting phases (austenite or ferrite). Another important goal is to reveal the chemical composition of the κ-phase as a function of isothermal annealing temperature using atom probe tomography (APT) and aberration-corrected scanning TEM (STEM).

* Corresponding author. Tel.: +82 54 279 2139; e-mail: cgpark@postech.ac.kr

1359-6462/$ - see front matter © 2012 Acta Materialia Inc. Published by Elsevier Ltd. All rights reserved.
http://dx.doi.org/10.1016/j.scriptamat.2012.08.013

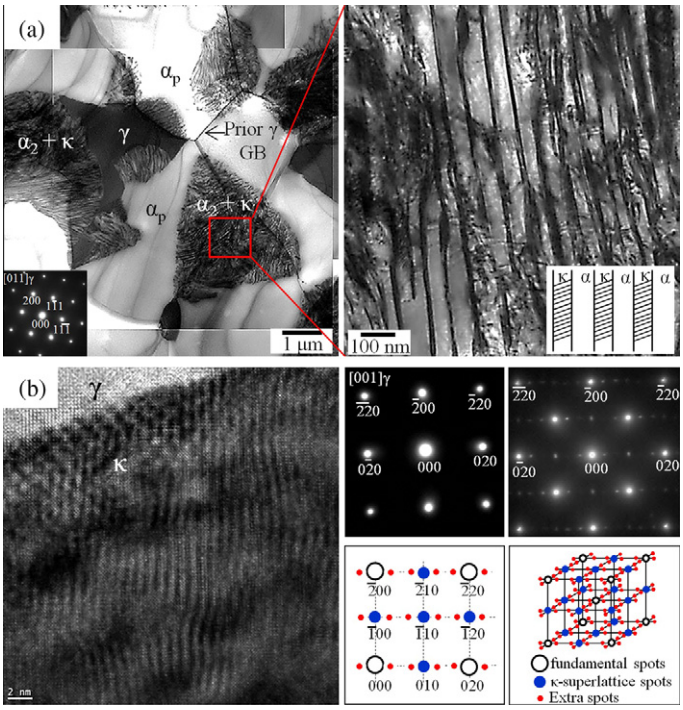

Figure 1. (a) TEM micrographs and the corresponding SADP taken from austenite for the steel subjected to isothermal holding at 500 °C. (b) HREM image and the corresponding SADPs of $[001]_\gamma$ zone including the simulated 2-D and 3-D reciprocal lattice illustrations of the perovskite κ-phase. α_p, polygonal ferrite; α_2, fine ferrite surrounded by carbides; γ, retained austenite; κ, κ-carbide.

2. Experimental procedure

An alloy with the composition 1.2 C, 3.2 Mn and 10.0 Al (at.%) was prepared by vacuum induction melting at 1200 °C for 60 min. Details of the alloy preparation and the thermomechanical processing have been published elsewhere [14]. In the current study, the cold-rolled steels were subjected to a two-step isothermal annealing: intercritical annealing at 900 °C for 30 min in a protective Ar atmosphere followed by isothermal annealing at 500 or 600 °C for 60 min and water quenching. The cooling rate from 900 °C to a desired level of holding temperature was about 150 K s^{-1} [6]. Microstructure characterization was done by TEM (JEM 2010F) and selected-area diffraction pattern (SADP) analysis. The TEM samples were prepared by electrochemical polishing. The lattice parameters of the κ-phase and the austenite were determined by high-resolution TEM (HRTEM). The chemical composition of the κ-phase was determined by energy-dispersive spectroscopy (EDS) on a Cs-corrected STEM (JEM 2100F) and APT. APT specimens were prepared by the standard two-stage electropolishing method. Prior to APT measurements, APT samples were also observed by TEM. APT analyses were conducted using a laser-assisted wide-angle APT (LAWATAP™, Cameca Instruments), applying laser pulses of 525 nm wavelength, 0.3 nJ pulse energy and 100 kHz pulse repetition rate at 40 K specimen temperature [15].

3. Results and discussion

Figure 1a shows TEM micrographs and SADP of the steel after an intercritical annealing followed by isothermal holding at 500 °C. The final microstructure is composed of a polygonal ferritic matrix (α_p) and the lamellae formed along the prior γ grain boundaries. In the lamellar structure, there are three other phases: fine ferrite, κ-carbide and retained austenite (γ_R). Hence, the γ phase is partially decomposed into ferrite and needle-like κ-carbide ($\gamma \rightarrow \kappa + \alpha_2 + \gamma_R$). For clarity, the ferritic matrix and the fine ferrite surrounded by κ-carbides have to be differentiated from each other and are hence denoted as α_p and α_2, respectively. The distribution of the α_p grains is irregular and inhomogeneous, as the current alloy has a duplex microstructure consisting of α and γ at 900 °C. HRTEM imaging yields lattice parameters of 3.65 Å for γ_R and 3.72 Å for κ, which corresponds to a lattice misfit (δ) of about 1.88% (Fig. 1b). The estimated δ is consistent with previous works [9,16], confirming that the phase boundaries between γ_R and κ are coherent as shown in Figure 1b. In the SADP along the [001] zone axis, clear {100}, {110} and {120} superlattice reflections of the κ-phase are visible. The intensity difference of the diffraction spots observed for the κ-phase can be assigned to the perovskite-type structure rather than $L1_2$ structure (characteristic of the γ′ phase). The diffraction patterns for both structures are very similar except for the fact that no intensity difference between {100} and {110} spots was detected for the γ′ phase with randomly distributed C atoms. However, the intensity of {110} spots in Figure 1b is much stronger than that of {100} and {120} spots. Typically, for fully austenitic Fe–(20–30) Mn–5.0Al–2.8C (wt.%) alloys, a higher intensity for the {010} superlattice spots than for the {110} spots was observed, which was caused by an ordering process of interstitial C at the body-centered site of κ-phase

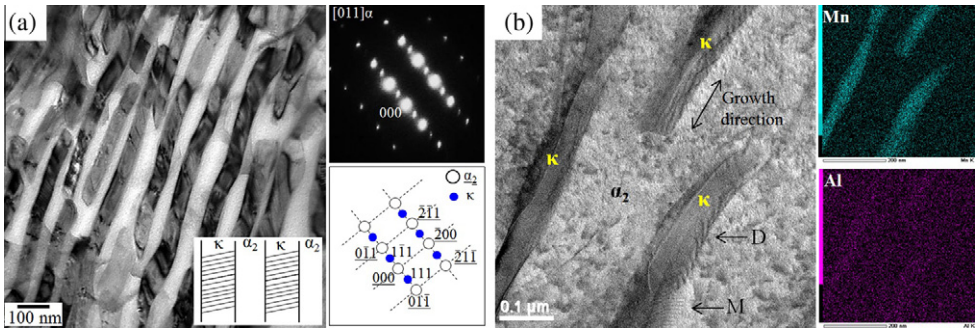

Figure 2. (a) TEM micrograph and the corresponding SADP of $[0\,1\,1]_\alpha$ zone for the steel isothermally annealed at 600 °C and (b) Cs-corrected (S)TEM bright-field image and the corresponding EDS elemental maps. D, dislocations; M, moiré fringes.

[11,12]. The intensity difference between {1 0 0} and {1 1 0} reflections, observed here, is probably attributed to the formation of C-vacancy long-range ordering inside the κ-phase formed by the employed annealing conditions, which is often observed in MC-type carbides (M = Nb, V, Mo and W) with a B1 structure [17] and in perovskite-type Ti_3AlC with an $L'1_2$ structure [18]. Furthermore, the SADP in Figure 1b reveals that there are several additional spots besides the fundamental and κ-carbide reflections. To date, this type of spot has not been found in Fe–Mn–Al–C alloys. We propose that the additional spots can be caused by fourfold splitting of the diffuse short-range order intensity peak. A similar splitting behavior was found in a disordered Cu_3Au alloy [19]. The origin of such splitting in this study could be due to an exchange of atomic position among Al, Fe and Mn inside the $L'1_2$-structure at elevated temperatures and the nominal composition of specimen.

TEM micrographs and the corresponding SADP with a $[0\,1\,1]_\alpha$ zone axis for the steel isothermally annealed at 600 °C are shown in Figure 2. In this specimen, γ phase is fully decomposed into κ-carbide and α_2 ($\gamma \rightarrow \kappa + \alpha_2$). The thickness or width of κ-particles increases with a higher annealing temperature: the average widths of the κ-particles at 500 and 600 °C are 17 ± 7 nm and 45 ± 10 nm, respectively. Thus, the spacing width between the particles for 600 annealed sample is lager than that of 500 sample due to a nucleation-growth process, leading to a decrease in the aspect ratio of the κ-particles. The shape of the κ-phase changes from extremely elongated rod-type to cylindrical-type as the annealing temperature increases. The elongated rod-like κ-carbides may be a result of high lattice misfit (δ) between α_2 and κ. The SADP confirms a $(0\,1\,1)_\alpha$ // $(1\,1\,1)_\kappa$ orientation relationship between the α_2 and κ-carbide, which corresponds to the well-known Nishiyama–Wasserman relationship [14]. Here, we observe that only {1 1 1} superlattice reflections for κ-phase are present without {1 1 0} spots for κ-phase. Assuming that the planar spacing of the $(1\,1\,0)_\alpha$ planes is 2.03 Å, the measured δ between α_2 and κ is nearly 5.9%, which implies that the formation of a coherent interface would be difficult. For such a high misfit value, the morphology of the precipitates was reported to be controlled by the elastic coherency term rather than by the interfacial energy contribution [11]. According to their results [11], the preferential growth of κ-carbide could be due to an increase in the elastic lattice misfit between γ and κ with

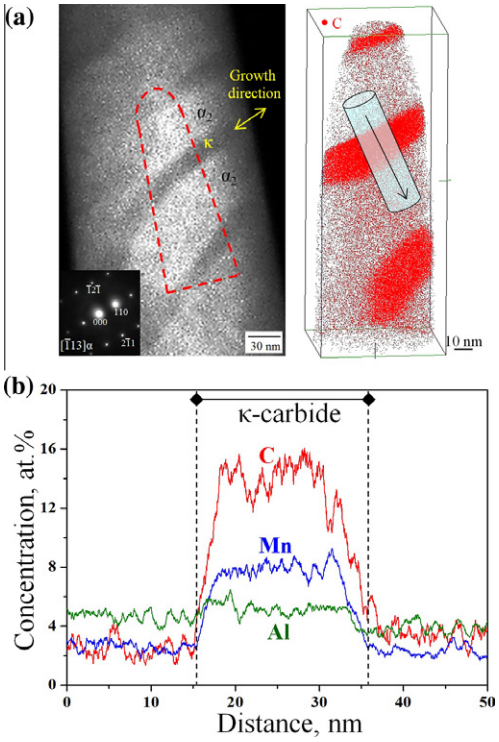

Figure 3. TEM image of APT specimen showing the lamellae formed in the steel after isothermal transformation at 600 °C and the corresponding SADP taken from ferrite, and the reconstructed APT map of C (red). The joint analysis including 1-D concentration profiles of elements obtained from the cylindrical region (cyan) reveals solutes partitioning and the morphology of the κ-carbides (For interpretation of the references to colour in this figure legend, the reader is referred to the web version of this article.).

aging time. The STEM image illustrates misfit dislocations (marked by "D") located at the α_2/κ interfaces given by Figure 2b, suggesting that the lateral interfaces are semicoherent. The spacing between dislocations dispersed at the interface is about 16.8 nm. The STEM-EDS maps reveal partitioning of Mn (cyan) and Al (pink) to κ-carbides. Although the Mn signals from the carbides are strong, the corresponding Al signals can barely be distinguished from those of the matrix. This means that the partitioning of Mn differs from that of Al. No significant C signals are also detected inside the carbides due to the insufficient sensitivity of STEM [20].

Figure 3 shows a TEM micrograph and the corresponding APT map of C (red) for the sample isothermally annealed at 600 °C. The two images were taken from exactly the same position as indicated. C-enriched lamellae are found in the reconstructed APT data, which can clearly be identified as κ-carbides by correlating the TEM micrograph with the APT map. Using 1-D composition profiles perpendicular to the semicoherent interfaces, the partitioning of solutes can be quantified. We detect a compositional fluctuation of C inside a κ-particle, much higher than those of Mn and Al. There are two possible explanations for this observation. (i) The observed C variation could be due to the formation of C-vacancies inside the κ-carbide. This defected state is in the following expressed as $(Fe,Mn)_3Al(C,Va)_x$. The stability of C–V formation inside the κ-carbide is also supported by thermodynamic calculations [7]. (ii) The preferential field evaporation induced by laser or voltage pulses and the trajectory overlap of the field-evaporated ions can lead to errors in measuring the absolute composition values determined by APT [21,22]. In this context and considering the enhanced intensity of {1 1 0} reflections in the SADP (see Fig. 1b), the former effect is more plausible than the latter one. Besides C atoms, Al and Mn atoms are partitioned to the κ-carbides, where the κ to α_2 ratio for Al is much lower than that for Mn, in good agreement with the EDS result (see Fig. 2b).

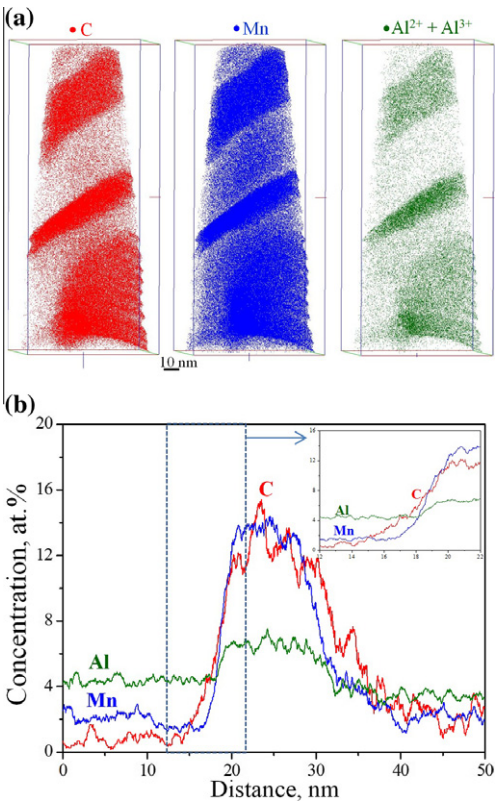

Figure 4. (a) APT maps of C, Mn (blue) and Al (green) for the steel after isothermal transformation at 500 °C, showing the rod-like shape of the κ-particles. Only 50% of Al atoms assigned as $^{27}Al^{2+}$ peak and $^{27}Al^{3+}$ peak are displayed. (b) Local concentration profiles of solutes and the artificial spread of planar interface in the vicinity of the κ/α_2 interface (For interpretation of the references to colour in this figure legend, the reader is referred to the web version of this article.).

Table 1. Chemical compositions of κ-carbide determined by APT and (S)TEM-EDS (in at.%).

Methods	APT		(S)TEM-EDS	
Temp.	500 °C	600 °C	500 °C	600 °C
Mn	14.4 ± 0.4	8.4 ± 0.4	12.7 ± 1.2	8.8 ± 0.7
C	12.8 ± 0.8	14.5 ± 1.0	–	–
Al	9.5 ± 0.2	10.1 ± 0.3	7.7 ± 0.9	7.6 ± 0.7

Table 2. The values of the enrichment factor (ε) between κ-carbide and α_2-ferrite for alloying elements as determined by APT.

	Mn	C	Al
500 °C	7.6	7.1	1.7
600 °C	2.8	4.8	1.2

The reconstructed C, Mn and Al maps obtained from APT for the steel annealed at 500 °C are shown in Figure 4. The needle-like shape of the κ-particles is confirmed. Nevertheless, APT artifacts that arise because of field-evaporation differences, such as a local magnification or demagnification effects [23,24], can lead to an error in measuring interfacial width between κ-particle and ferrite. For this reason, it is not possible to conclude unambiguously from the voltage-pulsed or laser-pulsed APT data whether the κ-phase is formed via spinodal decomposition or via a nucleation-growth sequence. Another point observed in this study is that decomposition of γ into κ and α_2 leads to supersaturation of α_2 with C.

The experimentally obtained concentrations of the κ-phase as a function of holding temperature are listed in Table 1. The Al content inside the κ-phase measured by APT was corrected by applying a deconvolution procedure for the overlapping Al^+ and Fe^{2+} mass peaks at 27 Da, considering the isotope ratios of Fe [6,25]. Accordingly, the C contents of κ-phase were obtained using the identification procedure for C peaks, as described in Ref. [26]. The compositional changes of the κ-phase depending on the temperatures as determined by APT are consistent with STEM-EDS data. In particular, an increase in the annealing temperature leads to a remarkable decrease in the Mn content of κ-carbide. This means that a higher annealing temperature affects the formation energy, lattice parameter and magnetization of κ-phase, as shown using density functional theory calculations [27]. Thus, we anticipate that an increase in the Mn substitution for Fe makes the κ-phase harder and stronger owing to the Mn–C atomic bonds being stronger than the Fe–C bonds.

Here, we confirm the formation of non-stoichiometric κ-carbides in Fe–Mn–Al–C alloys, in agreement with previous reports on κ-carbides existing over a range of varying Mn and Al contents [8,11–13]. According to these reports, the chemical composition of the κ-phase varies with both the nominal composition of the bulk specimen and its formation temperature. So far, the stoichiometric κ-phase has not been observed experimentally [28] and has been only theoretically addressed using ab initio calculations [27–29]. From our observations, we suggest under-stoichiometry of the κ-carbide with respect to C at the body-centered sites and partial replacement of Al by Fe or Mn in the corner positions

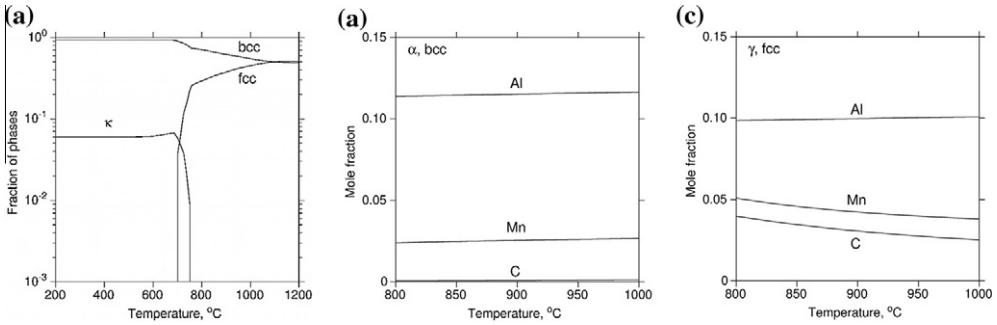

Figure 5. (a) Equilibrium phase fractions for the present alloy as a function of temperatures, and equilibrium concentration values of alloying elements in (b) ferrite and (c) austenite, as calculated using Thermo-Calc [7].

in its face-centered cubic-based unit cell. Thus, the composition of the κ-phase can be expressed as $(Fe,Mn)_3(Fe,Al)C_x$, but still containing Al. Partitioning of solutes to different phases can be quantified in terms of an enrichment factor, $\varepsilon = (\text{at.\% in } \kappa\text{-carbide})/(\text{at.\% in } \alpha_2\text{-ferrite})$. The ε values measured by APT are shown in Table 2. On the other hand, ε for Al is substantially lower than for Mn and C. It seems that Al is energetically stable inside either intermetallic κ or α_2 phase. Therefore, we conclude that during γ decomposition into κ and α_2, both product phases are competing sites for Al. This is an indication that the partitioning of Mn and Al to κ-carbides can be controlled by the abutting phase which is either austenite or ferrite.

We used Thermo-Calc predictions [7] to evaluate the remarkable decrease in ε for Mn and C with higher annealing temperature for the present alloy (Fig. 5). This calculation shows the equilibrium phase fractions of α and γ as a function of temperature. It confirms our microstructure characterization made above, namely the irregular and inhomogeneous distribution of α_p grains, as the current alloy has a duplex microstructure of α and γ at 900 °C. In addition, we quantify the concentration values of the elements in α and γ as a function of temperature, showing that most of the C can be solved in the γ, where the measured partitioning ratios of α to γ at 900 °C are 1.2/1.0 for Al and 1.0/2.0 for Mn, respectively. Even though Al is a strong ferrite former, a considerable amount of Al is solved in the γ phase at 900 °C. During isothermal holding at 500 or 600 °C for 60 min, the diffusion of C inside the γ phase is fast, while the diffusion of Al and Mn is negligible. Therefore, we propose that both the high content of Al partitioned to γ at 900 °C and fast diffusion of C during isothermal holding are significant factors for the nucleation of the κ-phase, leading to an accelerated decomposition of the γ phase. As reported, an ordering in Fe–Mn–Al–C alloys may be accomplished by the cooperative ordering of C and Al [30].

The compositional differences of κ-carbide grown at different holding temperatures can be understood in terms of undercooling (ΔT_1) between the intercritical temperature (900 °C) and the isothermal holding temperature (500 or 600 °C in this case). Stronger undercooling ($\Delta T_1 = 900\,^\circ\text{C} - 500\,^\circ\text{C}$) for the steels held at 500 °C leads to an increase in the driving force for pro-eutectoid ferritic transformation, reducing the γ fraction. As a result, a decrease in the γ fraction leads to an increase in the content of Mn and C in the γ phase and hence to its stabilization. To validate this, the volume fractions of the corresponding phases were determined by optical microscopy (OM), SEM, X-ray diffraction (XRD) and electron backscatter diffraction (EBSD). It is important to note that for the current alloys there are no ordered ferritic phases, such as B2 and DO3. Further OM, SEM and XRD results as shown in Figures S1 and S2 in the Supplementary Information confirmed that a higher holding temperature leads to a decrease in the γ_R fraction with increasing lamellae that are a mixture of fine ferrite and needle-like κ-carbide. The average volume fraction of the γ_R was 13.7 ± 2.0 vol.% and 4.8 ± 1.7 vol.% for the steels annealed at 500 and 600 °C, respectively. Based on the equilibrium phase fractions at 900 °C shown in Figure 5a, the pro-eutectoid ferrite fraction was also estimated as ~38 vol.% for 500 °C steel and ~56 vol.% for the 600 °C sample. It is therefore plausible that the steel annealed at 500 °C contains a higher γ_R fraction than the sample annealed at 600 °C, and that the κ-phase grown at 500 °C has a higher Mn and a lower Al content.

The morphological evolution of κ-carbide for different isothermal holding temperatures can be explained by the difference between the κ-phase precipitation-start temperature (750 °C as shown in Fig. 5c) and the respective holding temperatures. A stronger undercooling ($\Delta T_2 = 750\,^\circ\text{C} - 500\,^\circ\text{C}$) for the steel annealed at 500 °C increases the driving force for κ-phase precipitation, leading to a higher nucleation density of κ-particles. Subsequently, during isothermal annealing at 500 °C, the γ decomposition kinetics into κ-carbide is retarded due to the lower diffusion rate of solutes, especially C, compared to the 600 °C sample. Consequently, the κ-phase formed at 500 °C exhibits a finer and more dense distribution compared to that formed at 600 °C (Figs. 1 and 2). Here, it is the diffusion of C during isothermal holding that mainly controls κ-carbide morphology, whereas the contributions of Al and Mn are negligible.

4. Conclusions

We found direct evidence for the precipitation of nonstoichiometric κ-carbide, $(Fe,Mn)_3(Fe,Al)C_x$ containing Al, in a ferritic-matrix-based high-Al steel isothermally annealed at either 500 or 600 °C. With

increasing isothermal holding temperature: (i) the kinetics for γ decomposition increases; (ii) the width of κ-phase increases; (iii) the Mn content in κ-carbide decreases; and (iv) the enrichment factors for solutes decrease. We revealed that fine lamellae consisting of α_2 and κ-phase are formed by a eutectoid decomposition of γ, where the kinetics is controlled by the undercooling. Using TEM and APT, we also elucidated the solute partitioning at the atomic-scale and thus obtained insights into the transformation mechanism of the κ-phase in the ferrite matrix. Al atoms partitioned to austenite at high temperatures as well as the diffusion of C are significant factors for needle-like κ-carbide nucleation. The variable chemical composition of the κ-carbides was found to depend on the annealing temperature, which was confirmed by thermodynamic calculations.

Acknowledgements

The authors are grateful to Prof. D.W. Suh (GIFT) for careful reading and fruitful comments. We also acknowledge the help of H.J. Lee, J.H. Lee, Mr. H.S. Park, Prof. B.J. Lee (POSTECH), and Dr. I. Gutierrez, Dr. M. Friak (MPIE). This study was supported by POSCO and BK21.

Appendix A. Supplementary data

Supplementary data associated with this article can be found, in the online version, at http://dx.doi.org/10.1016/j.scriptamat.2012.08.013.

References

[1] D.W. Suh, S.J. Park, C.S. Oh, S.J. Kim, Scripta Mater. 57 (2007) 1097.
[2] D. Raabe, D. Ponge, O. Dmitrieva, B. Sander, Scripta Mater. 60 (2009) 1141.
[3] J.M. Jang, S.J. Kim, N.H. Kang, K.M. Cho, D.W. Suh, Met. Mater. Int. 15 (2009) 909.
[4] K.Y. Choi, C.H. Seo, H.C. Lee, S.K. Kim, J.H. Kwak, K.G. Chin, K.T. Park, N.J. Kim, Scripta Mater. 63 (2010) 1028.
[5] O. Dmitrieva, D. Ponge, G. Inden, J. Millan, P. Choi, J. Sietsma, D. Raabe, Acta Mater. 59 (2011) 364.
[6] J.B. Seol, D. Raabe, P. Choi, Y.R. Lim, C.G. Park, Acta Mater. (2012), http://dx.doi.org/10.1016/j.actamat.2012.07.064
[7] K.G. Chin, H.J. Lee, J.H. Kwak, J.Y. Kang, B.J. Lee, J. Alloys Compd. 505 (2010) 217.
[8] G. Frommeyer, U. Brüx, Steel Res. Int. 77 (9–10) (2006) 627.
[9] K.H. Han, J.C. Yoon, W.K. Choo, Scripta Metall. 20 (1986) 33.
[10] K. Sato, K. Tagawa, Y. Inoue, Scripta Metall. 22 (1988) 899.
[11] W.K. Choo, J.H. Kim, J.C. Yoon, Acta Mater. 45 (1997) 4877.
[12] K. Ishida, H. Ohtani, N. Satoh, R. Kainuma, T. Nishizawa, ISIJ Int. 30 (1990) 680.
[13] Y. Kimura, K. Handa, K. Hayashi, Y. Mishima, Intermeallics 12 (2004) 607.
[14] S.Y. Han, S.Y. Shin, H.J. Lee, B.J. Lee, S.H. Lee, N.J. Kim, J.H. Kwak, Metall. Mater. Trans. A (2011), http://dx.doi.org/10.1007/s11661-011-0942-2.
[15] T.M. Chen, T. Ohkubo, M. Kodzuke, K. Morita, K. Hono, Scripta Mater. 61 (2009) 693.
[16] A. Inoue, Y. Kojima, T. Minemura, T. Masumoto, Metall. Trans. A 12A (1981) 1245.
[17] J.H. Jang, C.H. Lee, Y.U. Heo, D.W. Suh, Acta Mater. 60 (2012) 208.
[18] C.S. Han, Met, Mater. Int. 14 (2008) 151.
[19] H. Reichert, S.C. Moss, K.S. Liang, Phys. Rev. Lett. 77 (1996) 4382.
[20] J.B. Seol, G.H. Gu, N.S. Lim, S. Das, C.G. Park, Ultramicroscopy 111 (2011) 623.
[21] A. Vella, F. Vurpillot, B. Gault, A. Bostel, A. Menand, B. Deconihout, Phys. Rev. B 73 (2006) 165416.
[22] F. Vurpillot, B. Gault, A. Vella, M. Bouet, B. Deconihout, Appl. Phys. Lett. 88 (2006) 094105.
[23] O. Thuillier, F. Danoix, M. Gouné, D. Blavette, Scripta Mater. 55 (2006) 1071.
[24] M.D. Mulholland, D.N. Seidman, Microsc. Microanal. 17 (2011) 950.
[25] O. Dmitrieva, P. Choi, S.S.A. Gestl, D. Ponge, D. Raabe, Ultramicroscopy 111 (2011) 623.
[26] Y.J. Li, P. Choi, C. Borchers, Y.Z. Chen, S. Goto, D. Raabe, R. Kirchheim, Acta Mater. 59 (2011) 3965.
[27] J.Y. Noh, H. Kim, J. Kor, Phys. Soc. 58 (2011) 285.
[28] D. Connétable, P. Magis, Intermetallics 16 (2008) 345.
[29] H. Ohtani, M. Yamano, M. Hasebe, ISIJ Int. 44 (2004) 1738.
[30] K.H. Han, W.K. Choo, Scripta Metall. 17 (1983) 281.